Nuclear Instruments and Methods in Physics Research A 767 (2014) 26–33

Contents lists available at ScienceDirect

Nuclear Instruments and Methods in Physics Research A

journal homepage: www.elsevier.com/locate/nima

Beam injection with pulsed multipole magnet at UVSOR-III

N. Yamamoto [a,*], H. Zen [b], M. Hosaka [a], T. Konomi [d], M. Adachi [c], K. Hayashi [d], J. Yamazaki [d], Y. Takashima [a], M. Katoh [d]

[a] Synchrotron Radiation Research Center, Nagoya University, Furo-cho, Chikusa-ku, Nagoya, Aich 464-8603, Japan
[b] Institute of Advanced Energy, Kyoto University, Gokasho, Uji, Kyoto 611-0011, Japan
[c] High Energy Accelerator Research Organization, KEK 1-1 Oho, Tsukuba, Ibaraki 305-0801, Japan
[d] UVSOR, Institute for Molecular Science, 38 Nishigo-Naka, Myodaiji, Okazaki 444-8585, Japan

ARTICLE INFO

Article history:
Received 10 June 2014
Received in revised form
26 July 2014
Accepted 29 July 2014
Available online 14 August 2014

Keywords:
Electron storage ring
Beam injection
Storage ring

ABSTRACT

In this study, we designed and manufactured a pulsed multipole magnet for beam injection into the UVSOR-III ring. A sextupole-like magnetic field could be excited when using the multipole magnet. To compensate for the residual field at the center of the magnet caused by manufacturing imprecisions, thin ferrite sheets were used. The injection experiments at UVSOR-III demonstrated multi-turn injections with the pulsed multipole magnet. The injection efficiency was 23% and the electron beam was stored up to the normal operation current of 300 mA. Moreover, we confirmed that oscillations of stored beams caused by beam injection were drastically suppressed compared with conventional pulsed dipole injection.

1. Introduction

The pulsed multipole injection scheme was developed at KEK-PF and KEK-AR [1,2]. In this scheme, the injection beam is captured into the accelerator acceptance as a result of pulsed multipole kicks, and the stored beam passes through the center of the multipole magnet, where the field strength is almost zero. The scheme thus avoids exciting coherent oscillation in the stored beam and delivers a high-quality photon beam for synchrotron radiation users.

The KEK group developed the qaudrupole and sextupole type magnets and demonstrated to suppress the oscillation of the stored beam. At BESSY-II, the octupole type magnet was developed and the injection efficiency around 80% was obtained [3]. Recently the extensive beam dynamics have been studied for the MAX-IV storage ring [4–6].

For relatively small rings, such as UVSOR-III [7], the pulsed multipole injection scheme provides additional advantages. In conventional bumped injection, at least two pulsed dipole (bump) magnets are required, and the perturbed (bumped) orbit is quite long. UVSOR-III currently has three bump magnets at different straight sections, and the distance between the first and the third bump magnet is over one-fourth of the circumference. In contrast, only one pulsed magnet is required in the pulsed multipole scheme. This scheme thus minimizes the injection system and realizes additional straight sections for insertion devices or machine-improvement devices.

Another consideration is the “multiturn” effect during the magnet discharging, which needs to be considered when applying the pulsed multipole scheme to relatively small rings. In this case, the injection beam travels through several large-amplitude turns and is affected by nonlinear forces in the ring. In previous experiments conducted at KEK-PF and KEK-AR, injection beams were kicked less than third times [1,2]. At UVSOR-III, the number of kicks could not be reduced further than seven because the revolution period is three times less than that of KEK-PF and the pulse period of the magnet could not be shortened for technical and economic reasons. In this situation, we could not confirm whether the multipole injection method works; more complicated considerations are imposed to apply this scheme to UVSOR-III.

Furthermore, with pulsed multipole injection, the residual field at the magnet center, where the stored beam transits, should be minimized. The residual field is so sensitive to the position of the magnet assemblies that extremely accurate manufacturing is required, achieving which involves high costs. To address this problem, we developed a field-compensation technique in which a set of soft ferrites is applied to the pre-manufactured magnets.

In this paper, we report the design of the multi-turn pulsed multipole injection for the UVSOR-III storage ring and analyze its operation. The pulsed multipole magnet was modified by using the field-compensation technique and then used for multi-turn pulsed multipole injection.

* Corresponding author.
E-mail address: naoto@nagoya-u.jp (N. Yamamoto).

http://dx.doi.org/10.1016/j.nima.2014.07.059
0168-9002/

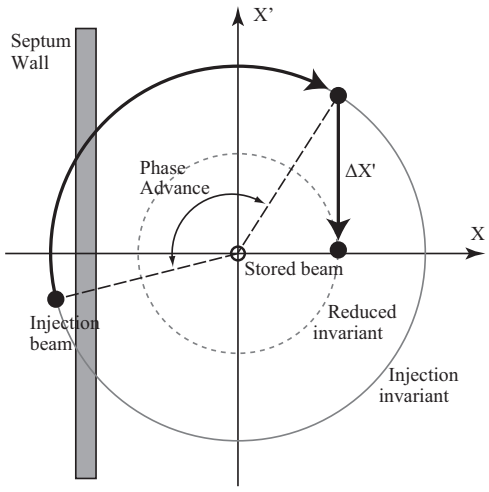

Fig. 1. Principle of pulsed multipole injection. Solid circles and open circle indicate injection beam and stored beam in phase-space, respectively.

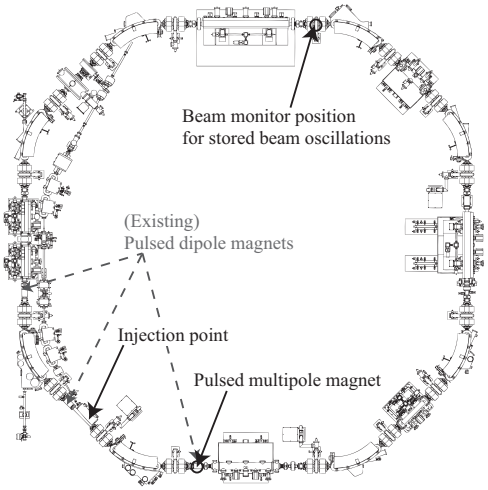

Fig. 2. Schematic image of the UVSOR-III storage ring.

2. Principle of pulsed multipole injection

The principle of pulsed multipole injection can be explained using Fig. 1, which shows the beam trajectories and the Courant–Snyder invariant in X–X' phase-space. The injection beam (solid circles) is transported from the exit of the septum magnet to the multipole magnet with a certain phase advance, while the invariant is maintained constant. At the multipole magnet, the injection beam receives the kick $\Delta X'$ and the invariant is reduced. When the reduced invariant, indicated by the dashed inner circle, is sufficiently smaller than the accelerator acceptance, the injection beam may be captured.

For convenience, we use the ratio of the reduced invariant to the accelerator acceptance as a dimensionless figure of merit (FOM) for the injection efficiency. It is defined as the ratio of the integrated areas, where a smaller ratio (i.e., a small FOM) indicates better injection efficiency. In contrast, the part of the injection beam with FOM >1 cannot be captured.

For the stored beam, indicated by the small open circle at the center of Fig. 1, the field strength of the multipole magnet is almost zero and coherent oscillations cannot be excited in the ideal case. In fact, the distribution of the stored beam should be considerable (see Fig. 2 in Ref. [2]).

3. UVSOR-III storage ring

UVSOR-III is an synchrotron light source at the Institute for Molecular Science in Okazaki, Japan. The accelerator complex was originally constructed as a second-generation VUV and soft x-ray source. The upgrades of 2003 [8] and 2012 [7] led to improved performance and qualified UVSOR-III as a third-generation source.

Top-up injection of the electron beam was started in 2010 to maintain a near constant beam current 300 mA during user experiments [9]. Because of the "close-bumped" orbit could not be realized due to poor magnet performance after the optics upgrades, the "open-bumped injection" scheme is now used for beam injection at UVSOR-III. Injecting the electron beam into the storage ring without using the closed bump orbit essentially requires kicking the stored beam horizontally, which induces betatron oscillations. These oscillations disturb user experiments and cause undesired spikes in the data. To solve this problem, we decided to use the pulsed multipole scheme instead of the conventional injection scheme.

Table 1
Main parameters of UVSOR-III storage ring for experiments.

Electron energy (MeV)	750
Circumference (m)	53.2
Revolution time (ns)	177
Natural emittance (nm rad)	16.9
Natural energy spread	5.4×10^{-4}
Horizontal tune	3.61
Vertical tune	3.26
Stored beam current	300 mA

Fig. 2 shows a schematic of the UVSOR-III storage ring, and Table 1 lists the main parameters. The electron energy is 750 MeV, and the circumference is 53.2 m. The lattice consists of four double-bend sections, four 4-m-long straight sections (long sections), and four 1.5-m-long straight sections (short sections). The beam emittance of 16.9 nmrad was achieved by distributing the dispersion function to all straight sections and by using combined-function dipole magnets [7]. The sextupole fields that serve to correct the chromaticity are introduced by the combined quadruple and dipole magnets. During the injection experiments, the storage ring was operated at the tune of $(\nu_x, \nu_y)=(3.61, 3.26)$, which is the designed operation point of the UVSOR-III ring.

The injection beam is provided by a 15 MeV-linac and a full energy booster synchrotron. During top-up, the injection rate is 1 Hz. An injection septum magnet, labeled as "injection point" in Fig. 2, is located at one of the short sections. For conventional dipole injection, three pulsed dipole magnets are used.

Numerical simulations indicate that only a few locations exist where the pulsed multipole injection scheme can be applied with adequate kick angle. We select the position about 4.42 m downstream from the injection point because it required the smallest kick angle for beam injection. The phase advance from the injection point to the location of the first kick was about 146°. In addition, an existing pulsed dipole magnet and a ceramic chamber were already located at this point. This configuration allowed us to examine the injection simply by replacing the magnet part; the vacuum system was not changed.

4. Construction of pulsed multipole magnet

4.1. Design of pulsed multipole magnet

Numerical calculations and cost studies led us to select a sextupole-like field. In ideal, a higher order field is more desirable

from the perspective of the field gradients around the center. Furthermore, in case of an even order multipole field, such as qaudrupole and octupole, the injection does not work because the sign of the second kick becomes opposite to the required one for UVSOR-III storage ring. In addition, the required load current for the sextupole-like magnet was reasonable for power supply manufacturing.

The magnet design should simultaneously obtain sufficient field strength for injection beams and negligible strength for stored beams. Small electromagnetic inductance is also important for the temporal response of the magnet. A magnet made of a rectangular shaped yoke and a one-turn coil satisfies these requirements. A small vertical gap fitted to the vacuum chamber is preferred because it provides greater field strength and a short single-turn coil is essential for reducing electromagnetic inductance.

In addition, we also aimed to minimize the residual field at the magnet center, which was caused by manufacturing imprecision, because the kick angle for stored beams is proportional to the residual field. To reduce the residual field, extremely accurate manufacturing is required. For the tolerance of the magnet performance, some methods were proposed [4,6]. We derived the tolerance to suppress the stored beam displacement to less than 10% of the beam size and a residual field within ± 0.5 mm from the magnet center to be less than 0.1 mT is required. This indicates that the required precision in the placement of each electrode coil was less than a few micro-ms. This requirement is difficult to be achieved by using normal manufacturing processes, whereby an electrode is fixed to the yoke material by using a resin insulator. In order to overcome these difficulties, we proposed a method to compensate the residual magnetic field by attaching thin ferrite sheets after a field measurement of pre-manufactured magnet.

4.2. Compensation of residual magnetic field

To compensate for the residual field, we used an electromagnetic interference (EMI) absorption sheet (MAB, Kitagawa Industries Ltd.), which is a thin flexible magnetic material with high resistivity. This EMI sheet is made of resin into which is incorporated a soft ferrite filler, and is available in thickness from 0.4 to 4.0 mm. Before inserting the EMI sheet, we measured the saturation magnetic-flux density as 0.338 T by using a vibrating sample magnetometer.

Fig. 3 shows a schematic of the magnet structures for the residual field-compensation technique for a sextupole-like magnet. Fig. 3(a) shows a 1-mm-thick EMI sheet on the outer side of the center coils, resulting in a uniformly increasing magnet field around the center. Fig. 3(b) shows the EMI sheet with the same thickness on the inner side, resulting in a uniformly decreasing magnetic field.

The field distribution calculated by the Poisson code [10] and the magnetic field measured by a Hall magnetic sensor are shown in Fig. 4. These data were measured for a pre-manufactured magnet, which is made by IDX Co., Ltd. without any EMI sheets, with dc 30 A at a vertical position of 0 mm and scaled to a current of 2.2 kA, where the field linearity up to 3 kA is confirmed by the Poisson code. The maximum magnetic field of 0.280 T at the ferrite position, where the vertical position is about ± 20 mm, was sufficiently low compared with the saturation magnetic flux density of the EMI sheet because the required kick is expected to be achieved for the current of 2.2 kA. In Fig. 4, the solid curve and open squares correspond to the original configuration (without EMI sheets), the dashed curve and open triangles correspond to the positive compensation configuration shown in Fig. 3(a), and the dot-dashed lines and open circles correspond to the negative-compensation configuration shown in Fig. 3(b). Within the range

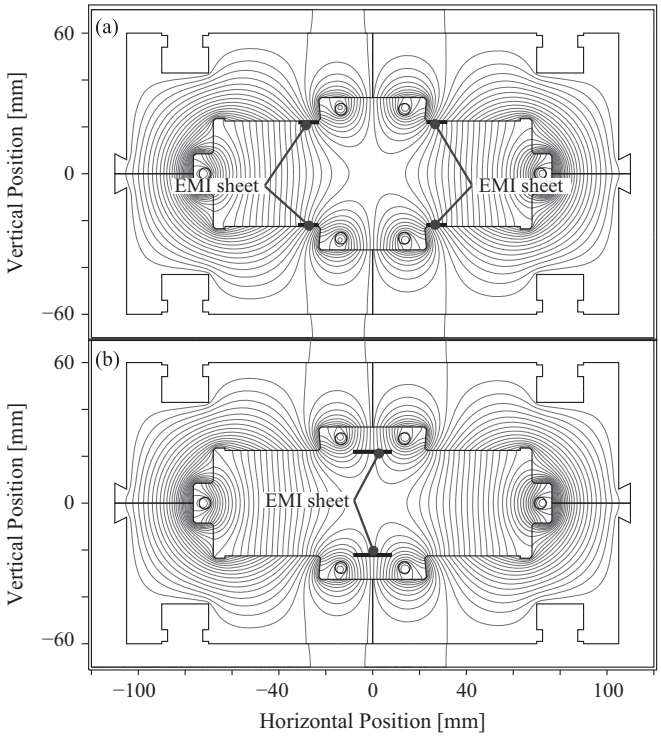

Fig. 3. Schematic of the multipole magnet compensated residual field. (a) Magnetic field shifts in the positive direction and (b) magnetic field shifts into the negative direction.

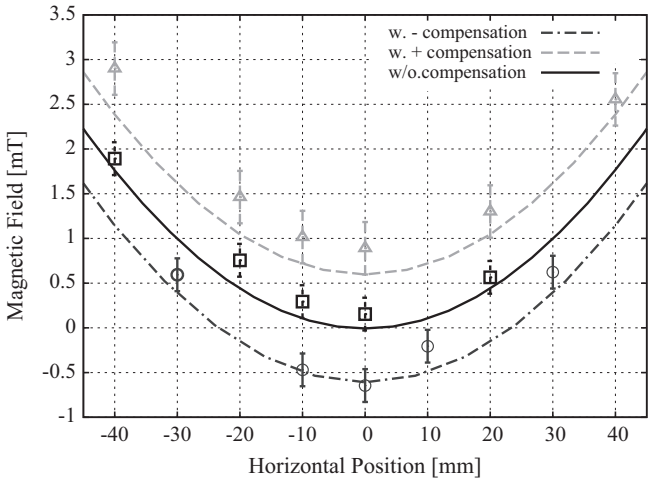

Fig. 4. Magnetic field distributions for three models of multipole magnets with the scaled current of 2.2 kA. The calculated results are shown by the three curves and the data are plotted with error bars. The measurements were performed at the vertical position of 0 mm in Fig. 3. The solid line and open squares indicate the multipole magnet without EMI field-compensation sheets. The dashed line and open triangles correspond to the positive compensation configuration shown in Fig. 3(a). The dot-dashed line and open circles correspond to the negative compensation configuration of Fig. 3(b).

of measurement error, the data reproduce the results of the calculation. We found that the magnetic field can be shifted ± 0.6 mT by using a 1-mm-thick EMI sheet. It should be noticed that the shifted value of the field depends strongly on the field strength and distribution at the location of EMI sheet. Then the situation described above is only one example by using 1-mm-thick EMI sheets for a sextupole-like magnet.

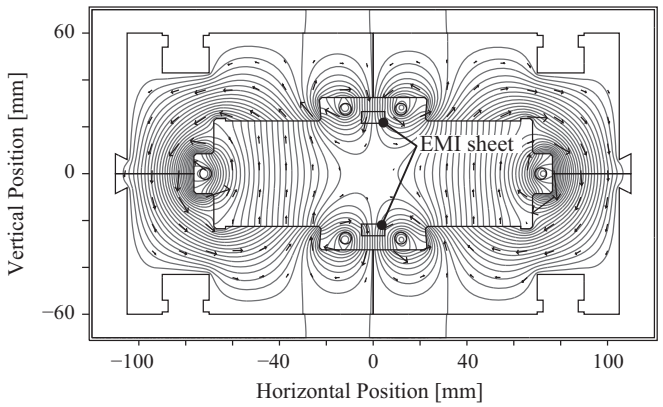

Fig. 5. Cross-section of manufactured multipole magnet with calculated field distribution. Open circles indicate the electrode coils and the two open squares indicate the EMI sheet that was introduced to compensate the error in the magnetic field.

Table 2
Parameters for the multipole magnet.

Sextupole magnet	
Iron yoke length	240 mm
Vertical gap	45 mm
Horizontal gap	136 mm
Magnet inductance	2.15 μH
York material	Laminated silicon steel (0.2 mm thick)
Power supply	
Max. peak current	2.4 kA
Max. charging voltage	22 kV
Pulse period	1.33 μs
Max. repetition rate	3 Hz

4.3. Manufacturing the magnet

Fig. 5 shows a cross-section of the multipole magnet on which the calculated field distribution is superimposed. The specifications of the magnet and the pulsed power supply are summarized in Table 2. The magnet yoke was made of 0.2-mm-thick laminated silicon steel sheets to reduce the effects of eddy currents. The open circles in Fig. 5 indicate the electrode coils and the coil is formed by a 5-mm-diameter single-turn copper bar. The iron yoke length and cross-sectional geometries were dictated by the shape of the ceramic chamber and the requirement of a 1-mm clearance. Two open squares represent the EMI sheets described in Section 4.2. The position and thickness (4.4 mm) of the EMI sheets were determined based on field measurements of the pre-manufactured magnet. The residual field of the pre-manufactured magnet was 4 mT. The measured inductance of the magnet was 2.15 μH, which is 35% greater than the calculated inductance. We considered that the connection parts of electrode coils contributed to this additional inductance.

Fig. 6 shows the horizontal distribution of the integrated field. The solid line indicates the integrated magnetic field evaluated by scaling the calculated magnetic field by the effective core length of 280 mm. The magnetic field was estimated by using the Poisson code and the effective core length was determined by measuring with a Hall magnetic sensor. The open circles indicate measurement data, which were measured at dc 30 A and scaled to the operating current of 2.2 kA. These results are less than the calculated results because the magnetic field around both edges is canceled by the magnetic field generated from the parts that connect the single-turn coil.

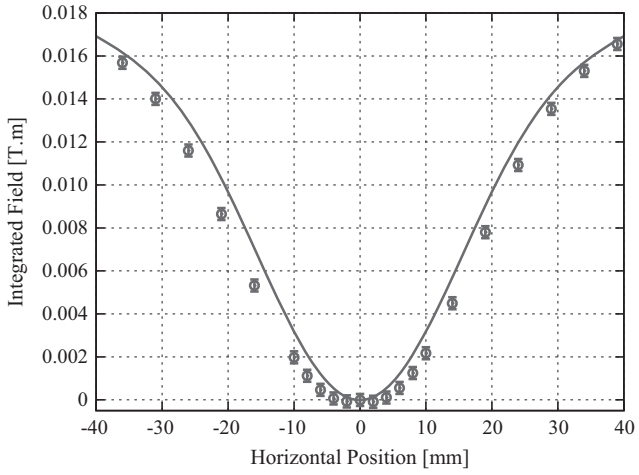

Fig. 6. Integrated magnetic field of the manufactured multipole magnet with the scaled current of 2.2 kA. The measurement was made with dc 30 A. The solid line is evaluated by multiplying the calculated magnetic fields by the effective core length. The measured values are plotted as open circles with error bars.

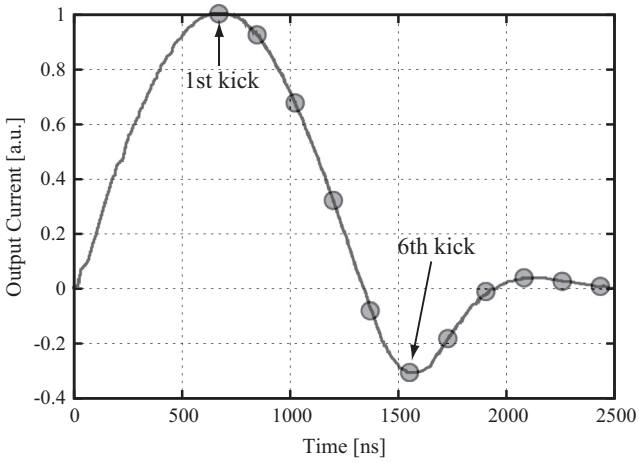

Fig. 7. Power supply output current monitored by a current monitor. Solid circles represent the kick timing when a beam is injected at the peak timing of discharging pulse.

The power supply was produced by IDX Co., Ltd. and installed near the multipole magnet. The connection cables with the pulser and magnet were 30 cm long. Fig. 7 shows the output current of the power supply as measured by a current monitor.

The power supply has a maximum charging voltage of 22 kV and produces a 2.4 kA output current in a half-sine pulse shape with a full width of 1.33 μs. A reflection current appears with an amplitude that is 30% the main peak. The estimated total inductance is about 4.0 μH, which is sum of the contributions from the magnet and the pulser circuit. The required peak current of 2.2 kA is achieved for a charging voltage of 19.7 kV. The maximum repetition rate is 3 Hz. No electric discharge between the EMI sheets and the electrode coils was observed during magnet operation.

For simple and efficient beam injection, the single-kick scheme is preferred. However, a period of revolution for the UVSOR-III storage ring is about 177 ns; thus, to create a pulse that is as short as two revolution period is difficult both technically and economically. For this reason, we used a pulse period of 1.33 μs. When the injection timing is tuned at the peak, the beam experiences more than seven kicks. The timing of the kicks for the injection beam is plotted as solid circles in Fig. 7.

5. Injection calculation

The SAD code [11] was used for beam-tracking simulations and the lattice model was modified by using measured parameters such as betatron tunes, chromaticities and a horizontal dispersion. In the tracking simulations, the field distribution calculated by the Poisson code was used as the field from the pulsed multipole magnet. Tune shifts determined by finite beam amplitudes and sextupoles for correcting the chromaticity were taken into the consideration.

The results of a six-turn tracking calculation and the acceptance ellipse at the location of the pulsed multipole magnet are shown in Fig. 8. An injection beam is generated from an injector with the emittance of 680 nmrad and an energy spread of 2.3×10^{-3}. It passes 40 mm horizontally from the central orbit of the ring at the injection point. The beam distribution at this point is plotted as green dots on the left inset of Fig. 8, in which the twiss parameters beta and alpha are assumed to be 1.5 m and 0 at the injection point, respectively. The twiss parameters beta and alpha at the pulsed multipole magnet location are 1.8 m and 0, respectively. In the calculation, the injection beam is represented by a thousand macro-particles with three-sigma Gaussian distribution in six-dimensional phase-space, and we assume that the injection timing for the magnet pulse is set on the peak of the discharge current (i.e., 660 ns in Fig. 7) and the output voltage of power supply is 22 kV, which corresponds the output current of 2.4 kA.

Calculated horizontal trajectory as a function of the longitudinal position and an estimated kick for the injection beam at each turn based on the pulsed multipole magnet are shown in Figs. 9 and 10, respectively. The arrows in Fig. 9 indicate the location of the pulsed multipole magnet at each turn. At the first turn, the injection beam has a horizontal amplitude of 35 mm and a divergence of 2 mrad. The kick angle for the first turn is calculated to be −6 mrad, and the invariant quantity increases because the kick is too strong. At the second turn, the beam with a horizontal amplitude of 19 mm and a divergence of 5.8 mrad experiences a kick of −2.6 mrad, and the reduced invariant becomes slightly smaller than the acceptance of the accelerator. Furthermore, the invariant quantity is also slightly reduced at the sixth turn, which corresponds to the reflection peak of the power supply (see Fig. 7). These results indicate that the first kick serves to adjust the phase advance for the second and sixth kicks.

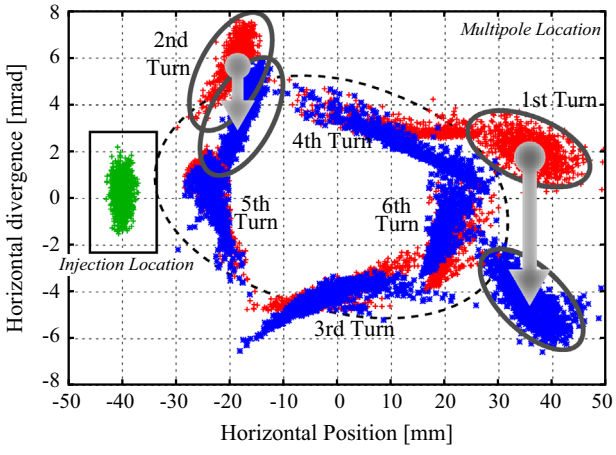

Fig. 8. Calculation of six-turn beam distribution in phase-space based on pulsed multipole injection at the output voltage of 22 kV. The initial distribution of the beam at the injection location is drawn in green. The beams before and after each turn's kick, which occurs at the multipole magnet, are drawn in red and blue, respectively. The beam trajectories of first and second kicks are emphasized by the using solid ellipses. The dashed ellipse represents the acceptance at the location of the pulsed multipole magnet. (For interpretation of the references to color in this figure caption, the reader is referred to the web version of this paper.)

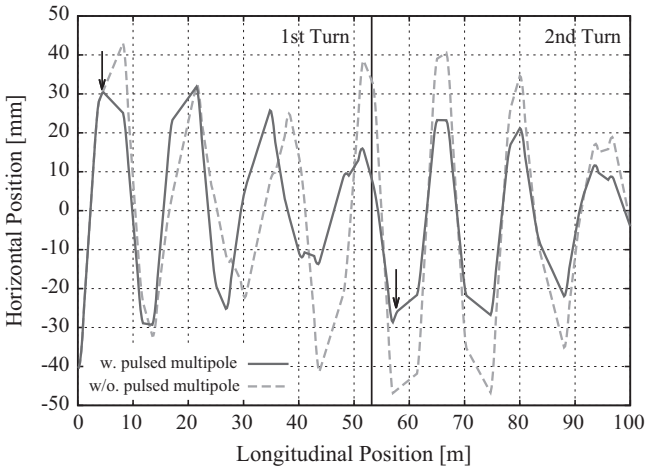

Fig. 9. Calculated Horizontal trajectory as a function of the longitudinal position for the pulsed multipole injection. The solid and dashed lines represent with and without pulsed multipole magnet, respectively. The arrows indicate the location of the pulsed multipole magnet at each turn.

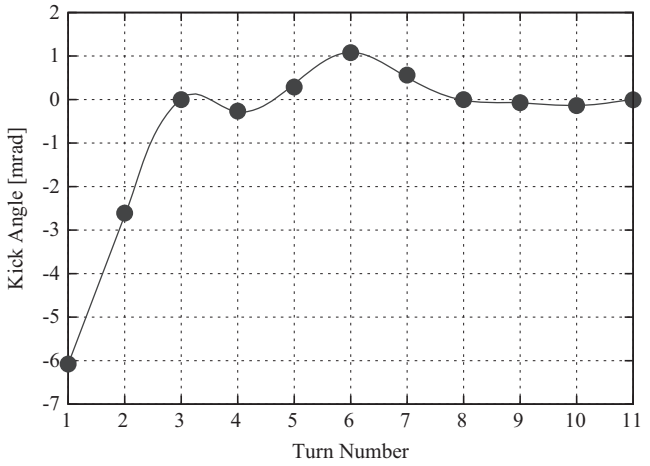

Fig. 10. Estimated kick angle provided by the pulsed multipole magnet for injection beam at each turn. The beam is assumed to be injected at the peak of the magnet pulse.

In addition, the effect for the sixth kick was expected by the beam tracking in the design process of the power supply and the requirement for the pulse shape was eased, which led the cost reduction of the power supply.

After the discharging pulse is dumped, the ratio of the reduced invariant to the accelerator acceptance (i.e., the FOM) becomes 0.46 for a center particle of the beam and the injection efficiency is estimated to be 65%. In comparison the resulting injection efficiency for the conventional dipole injection scheme is around 45%.

6. Results and discussions

6.1. Beam injection test

The injection efficiencies as functions of the injection timing and output voltage are plotted as solid circles in Figs. 11 and 12, respectively. A maximum injection efficiency of 23% was achieved with an injection timing of 600 ns and an output voltage of 22 kV, which correspond to a timing near the discharge peak of the pulse (see Fig. 7) and to the maximum output voltage. In this situation, we also injected the electron beam up to the normal operating

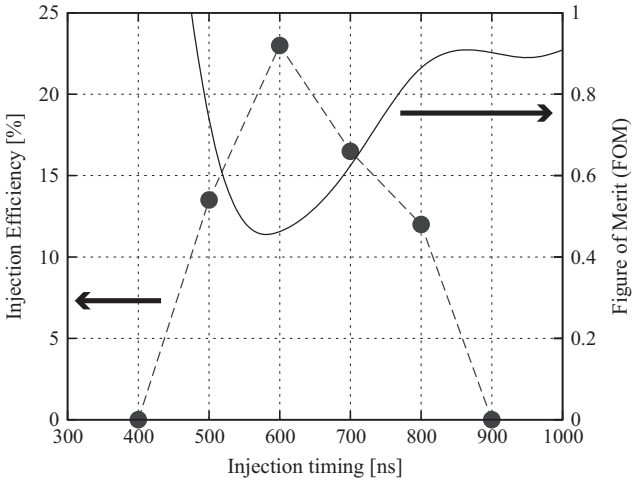

Fig. 11. Measured injection efficiencies as a function of the injection timing. The measurements were performed with the output voltage of 22 kV.

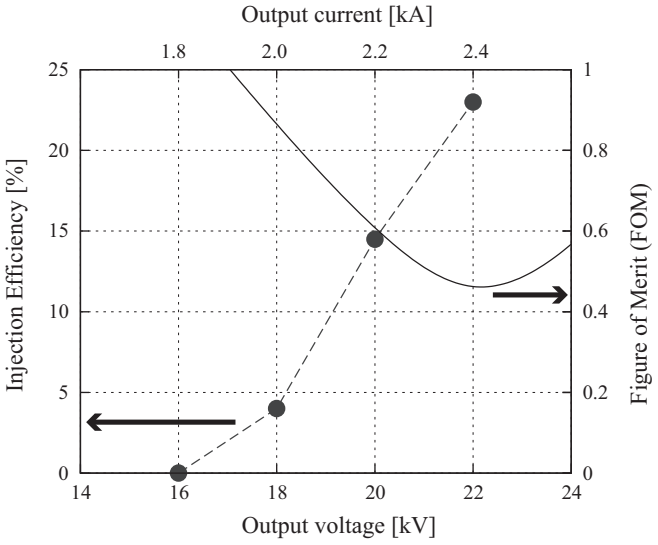

Fig. 12. Measured injection efficiencies as a function of the output voltage. The measurements were performed with the injection timing of 600 ns.

currents of 300 mA. However, the maximum injection efficiency was only one-third of what we estimated.

Figs. 11 and 12 show the measured injection efficiencies and the FOMs calculated by the beam-tracking simulation. The results indicate that the maximum injection efficiencies occur where the reduced invariant is minimum.

This indicates that the experimental results can be qualitatively understood by beam-tracking simulations. In the experiments, the power supply limited the output voltage to 22 kV; however, we do not expect better injection efficiencies for higher output voltages. If the output voltages are greater than 22 kV, the kick angle at first turn would increase but at the second turn would decrease because of the larger phase advance shift of the beam, and because the horizontal position of the beam approaches the magnet center. Then, the resulting reduced invariance becomes larger, and more particles would be lost.

The results of a six-turn tracking calculation for the output voltage of 26 kV are shown in Fig. 13. The kick angle at first turn increases and is calculated to be −8 mrad. At second turn, the beam with horizontal amplitude of 15 mm, which is slightly smaller compared with the same turn of 22 kV case shown in

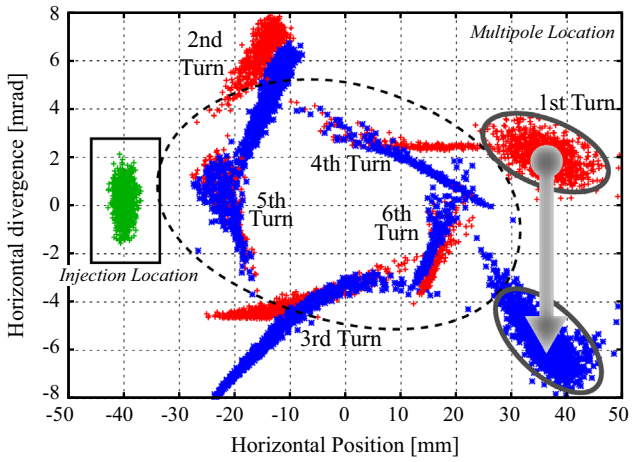

Fig. 13. Calculation of six–turn beam distribution in phase–space based on pulsed multipole injection at the output voltage of 26 kV. The initial distribution of the beam at the injection location is drawn in green. The beams before and after each turn's kick, which occurs at the multipole magnet, are drawn in red and blue, respectively. The beam trajectories of first kick are emphasized by the using solid ellipses. The dashed ellipse represents the acceptance at the location of the pulsed multipole magnet. (For interpretation of the references to color in this figure caption, the reader is referred to the web version of this paper.)

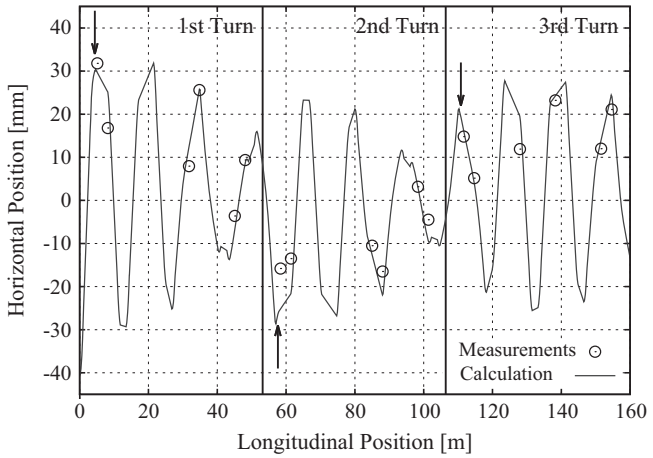

Fig. 14. Horizontal trajectory as a function of the longitudinal position for the pulsed multipole injection. The solid line and solid circles represent the calculated result and the data acquired using turn-by-turn beam-position monitors, respectively. The arrows indicate the location of the pulsed multipole magnet at each turn.

Fig. 8, experiences a weaker kick. Furthermore, at third turn, the beam has larger amplitude and more than half of the beam are kicked out of the acceptance and lost as a result of the kick. Then the injection efficiency become worse than the case of output voltage of the 22 kV. We show the calculation result for the output voltage of 26 kV for the explanation, the same consequences are obtained in the case for the greater output voltage than 22 kV. This means that the difference of the phase advance for the injection beam affects the injection efficiencies and it limits the flexibility of the ring optics. Especially for the multi-turn injection scheme, the amplitude-dependent tune shift is being changed with turn by turn according to the each kick angle. Then the flexibility of the operation tune is significantly limited.

The horizontal trajectory of the injection beam for the pulsed multipole injection was measured using turn-by-turn beam-position monitors [12] and is plotted, as shown in Fig. 14, along with the calculated trajectory. This plot shows that the injection conditions for the horizontal direction are reproduced by the calculation.

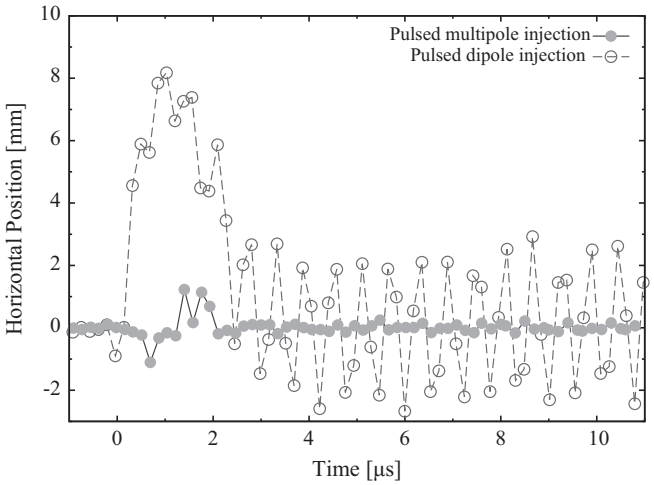

Fig. 15. Measured stored beam movements with pulsed dipole magnet (open circles) and pulsed multipole magnet (close circles).

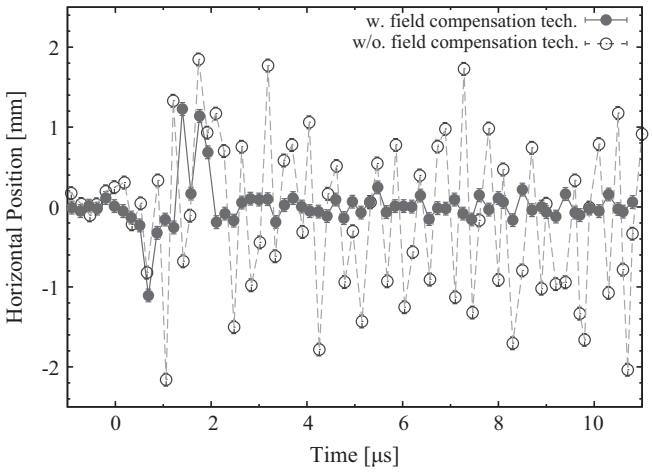

Fig. 16. Measured stored beam movements with (close circles) and without (open circles) field compensation technique for pulsed multipole magnet.

The discrepancies of the injection efficiency between the calculated and measured results are attributed to the injection beam qualities or unexpected nonlinear forces. In our calculation, the injection efficiency depends strongly on beam blurring in the phase-space. We considered only the sextupole field of the designed lattice and evaluated the FOM, including the off-center beam, to be 0.68 ± 0.4 for all particles. Note that particles with an invariant greater than 1 cannot be captured. If the quality of the injection beam decreases slightly or if additional nonlinear forces arise somewhere in the ring, the efficiency would drastically reduce.

6.2. Coherent oscillations of stored beams

Fig. 15 shows the horizontal displacements of the stored beam as a function of time for both the conventional pulsed dipole and the completed pulsed multipole. The measurement accuracy for the position was about 80 μm. The solid and open circles indicate the data of pulsed multipole and the conventional pulsed dipole, respectively. The beam position was measured about 31 m downstream from the injection point, as shown in Fig. 2, and both pulsed magnets were discharged at 0 μs. The horizontal betatron function at the monitor position is 7.4 m and the maximum betatron function of the ring is 7.6 m.

For the pulsed dipole case, the orbit was distorted and the beam underwent betatron oscillations with amplitudes of about 2 mm.

However, for the pulsed multipole case, although some spikes occurred for the same magnet discharge timing, no significant oscillations were observed after the discharge pulse. The spiky signals are attributed not to the stored beam but to the electric noise generated by the pulsed magnet. No observable coherent oscillation of stored beams occurred. Note that the estimated amplitude based on the measured field shown in Fig. 6 from beam-tracking simulations is 8 μm.

These results indicate that coherent oscillations of the stored beam are drastically suppressed on using pulsed multipole injection. It is considered that the betatron amplitude of 2 mm for the pulsed dipole reduced to at least 80 μm, which is the measurement accuracy, for the pulsed multipole. Then the reduction is estimated to be 96%.

Furthermore, for the pulsed multipole magnet, the horizontal displacement of the stored beam with and without the field-compensation techniques is shown in Fig. 16. The solid and open circles indicate the data with and without field compensations, respectively; the data corresponding to field compensation are the same as those in Fig. 15. Betatron oscillations beyond the beam position monitor resolution occurred only without the field compensation, and the amplitude of these oscillations is consistent with the calculated result based on a residual field of 4 mT (which was measured for pre-manufactured magnet). Therefore, these experiments demonstrate that the proposed field-compensation technique effectively cancels the residual field.

7. Conclusion

To introduce pulsed multipole injection into the UVSOR-III storage ring, we designed a rectangular-shaped pulsed multipole magnet and tested it for electron beam injection. The goal of the design was to compensate for residual magnetic fields by using thin ferrite sheets applied to the pre-manufactured magnet.

The injection experiments demonstrated that multiturn injection, which uses the pulsed multipole magnet, is successful technique for UVSOR-III. This is the successful result of the pulsed multipole injection in case of as many as 7–9 kicks being applied to the same injected bunch on consecutive turns.

After optimizing the injection conditions, we obtained a maximum injection efficiency of 23% and an electron beam injection up to 300 mA. The injection efficiency obtained was less than expected from beam simulations, but the efficiency was sufficient to maintain the top-up operation at 300 mA. We suggest that the quality of the injection beam may have caused the lower injection efficiency because an injection efficiency lower than expected also occurred when using conventional dipole magnets. Thus, to obtain a higher injection efficiency, we shall focus our future investigations on the injector system.

Finally, this work demonstrates that the field-compensation technique based on using thin ferrite sheets to cancel the residual magnet field is an economical and powerful way to improve performance. Coherent oscillations were drastically suppressed by applying this technique to pre-manufactured magnet that had a residual field of 4 mT. This compensation technique may also be applied to other types of pulsed magnets.

References

[1] K. Harada, Y. Kobayashi, T. Miyajima, S. Nagahashi, Physical Review Special Topics—Accelerators and Beams 10 (12) (2007) 123501. http://dx.doi.org/10.1103/PhysRevSTAB.10.123501.

[2] H. Takaki, N. Nakamura, Y. Kobayashi, K. Harada, T. Miyajima, A. Ueda, S. Nagahashi, M. Shimada, T. Obina, T. Honda, Physical Review Special Topics—Accelerators and Beams 13 (2010) 020705. http://dx.doi.org/10.1103/PhysRevSTAB.13.020705.
[3] T. Atkinson, M. Dirsat, O. Dressler, P. Kuske, H. Rast, Development of a Non-Linear Kicker System to Facilitate a New Injection Scheme for the bessy ii storage ring, 2011.
[4] S.C. Leemann, Physical Review Special Topics—Accelerators and Beams 15 (2012) 050705. http://dx.doi.org/10.1103/PhysRevSTAB.15.050705.
[5] S. Leemann, Nuclear Instruments and Methods in Physics Research Section A: Accelerators, Spectrometers, Detectors and Associated Equipment 693 (0) (2012) 117 http://dx.doi.org/10.1016/j.nima.2012.07.023, URL ⟨http://www.sciencedirect.com/science/article/pii/S0168900212007905⟩.
[6] S. Leemann, L.O. Dallin, Progress on pulsed multipole injection for the max iv storage rings, in: PAC'13 (2013 Particle Accelerator Conference), PAC'13 OC/IEEE, 2013, pp. 1052–1054.
[7] M. Adachi, H. Zen, T. Konomi, J. Yamazaki, K. Hayashi, M. Katoh, Journal of Physics: Conference Series 425 (4) (2013) 042013, URL ⟨http://stacks.iop.org/1742-6596/425/i=4/a=042013⟩.
[8] M. Katoh, K. Hayashi, T. Honda, Y. Hori, M. Hosaka, T. Kinoshita, S. Kouda, Y. Takashima, J. Yamazaki, Nuclear Instruments and Methods in Physics Research Section A: Accelerators, Spectrometers, Detectors and Associated Equipment 467–468 (Part 1) (2001) 68. http://dx.doi.org/10.1016/S0168-9002(01)00217-0, URL ⟨http://www.sciencedirect.com/science/article/B6TJM-43N61TY-P/2/512e845-bb5fa01f77a072106eced320c⟩.
[9] H. Zen, M. Adachi, M. Katoh, K. Hayashi, J. Yamazaki, T. Tanikawa, Y. Taira, M. Hosaka, N. Yamamoto, Status of top-up operation in uvsor-ii, in: Proceedings of the International Particle Accelerator Conference, Kyoto, 2010, p. 2576.
[10] Poisson/Superfish, Los Alamos National Laboratory Report No. LA-UR-96-1834.
[11] K. Oide, A final focus system for flat-beam linear colliders, Nuclear Instruments and Methods in Physics Research Section A 276 (1989) 427–432.
[12] A. Nagatani, Y. Takashima, M. Hosaka, N. Yamamoto, K. Takami, M. Katoh, M. Adachi, H. Zen, K. Hayashi, Development of turn-by-turn bpm system at uvsor-ii, in: UVSOR Activity Report 2009, vol. 1, UVSOR IMS, 2010, p. 34.